C h a p t e r 4

Catalytic transfer hydrogenation of N_2 to NH_3 via a photoredox catalysis strategy

Adapted from:

Johansen, C. M.†; Boyd, E. A.†; Peters, J. C. *Sci. Adv.* **2022**. 8, eade3510. DOI: 10.1126/sciadv.ade3510.

† These authors contributed equally to this work.

4.1 Introduction

Multi-electron reductive transformations of small molecule substrates (e.g., N_2, CO_2, NO_3^-) are challenging to mediate in homogeneous catalysis and most typically require considerable energy input via harsh chemical reagents and/or conditions to be driven forward. The nitrogen reduction reaction (N_2RR) offers a case in point; substantial progress has now been made in molecular catalyst design but significant overpotentials are generally needed to observe NH_3 product.[1,2,3] For nitrogen reduction (N_2R), kinetic challenges also prevail for enzymatic and heterogeneous catalysis that require substantial energy inputs, via ATP hydrolysis for the former and high temperature and pressure or electrochemical overpotential for the latter,[4,5,6] despite a thermally favorable Gibbs free energy of formation, $\Delta G_f(NH_3)$ (Figure 4.1A).

The organometallic catalysis field has pursued photochemical strategies as a means of driving small molecule reductions, with considerable success being achieved for CO_2 reduction (CO_2R, typically by 2 e^-/2 H^+) as the target transformation.[7,8] Such strategies are still challenged by the widespread use of sacrificial donors whose oxidation products are not readily recycled. While design schemes are envisaged to someday couple photodriven CO_2R catalysis with water oxidation, photodriven transfer hydrogenation using a suitable precatalyst offers an approach to reductive small molecule catalysis, especially if the net H_2-donor (H_2-carrier; Figure 4.1B) derives from a structure than can be efficiently recycled, for example via hydrogenation or electrochemically.

Reduced Hantzsch esters (HEH_2, Figure 4.1B) and chemically related structures (e.g., reduced acridine, phenanthridine) have been explored for thermally and photochemically driven reductive hydride (H^-; NADH-like) and H-atom transfers in organic synthesis.[9] Moreover, they are highlighted for their chemical (and electrochemical) recyclability via net hydrogenation of the spent pyridine-type oxidation product.[10,11] Whereas the types of transformations they participate in are most typically two-electron processes, they are also tempting to explore for deeper multi-electron reductions of the type pursued in small molecule reductive catalysis. Focusing on N_2R,[12] we noted that despite long known and still debated studies of photocatalytic nitrogen fixation using

semiconductors,[13,14,15] and photodriven N_2R mediated by nitrogenase coupled with CdS,[16,17] as yet there were no examples of photochemically driven catalytic N_2R using well-defined molecular systems. Hence, photoinduced N_2R via transfer hydrogenation from a Hantzsch ester or related donor, which requires the donors to engage in successive transfers to mediate a deep 6 e^-/6 H^+ reduction process, provides an excellent test case of this strategy for small molecule substrates.

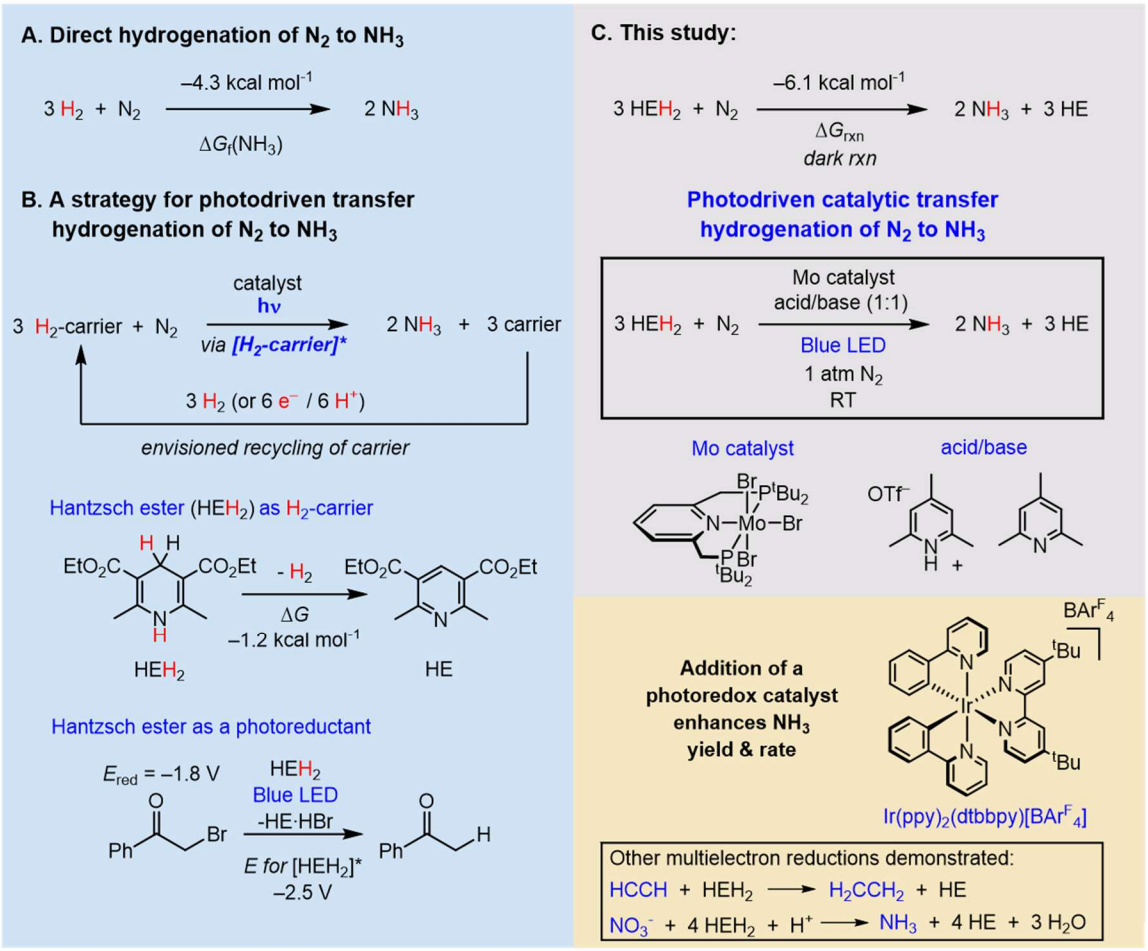

Figure 4.1. Thermodynamics and strategies for hydrogenation of N_2. (A) Thermodynamics of hydrogenation of N_2 to NH_3;[1] (B) Schematic of an overall design for light-driven transfer hydrogenation of N_2; chemical structure of the Hantzsch ester used in this study (HEH_2);[19] representative reduction of α-bromo acetophenone;[18] (C) Net stoichiometry and estimated driving force of transfer hydrogenation from HEH_2 to N_2 forming NH_3; photodriven (blue LED) process described in this study, in the absence and presence of a photoredox catalyst.

All thermochemical values are given in MeCN at 25 °C with ferrocenium/ferrocene ($Fc^{+/0}$) as reference potential.

Considering thermodynamic parameters relevant to the aforementioned goals, in its ground state the first C–H bond dissociation free energy ($BDFE_{C–H}$) of HEH_2 is 62.3 kcal $mol^{–1}$ in MeCN at 25 °C (all following thermochemical values are defined at these conditions), which is not weak enough to bimolecularly liberate H_2.[18] Photoexcitation of HEH_2, however, renders an excited state that is highly reducing (E_{ox} for $[HEH_2]^*$ is ~ –2.6 V vs $Fc^{+/0}$; Fc = ferrocene).[19,20] Photodriven (blue LED) reduction of α-bromo acetophenone to acetophenone by HEH_2 illustrates its capacity to deliver an H_2 equivalent (Figure 4.1B).[19] For a dark N_2R reaction, we estimate the overpotential for reduction of N_2 by HEH_2 to generate NH_3 as 1.8 kcal $mol^{–1}$ (($\Delta\Delta G_f(NH_3)$, Figure 4.1C). Using light (blue LED), we show herein that it is indeed possible to catalyze photoinduced transfer hydrogenation from HEH_2 to N_2 using Nishibayashi's molybdenum pre-catalyst (Figure 4.1C)[21] at atmospheric pressure and 23 °C. The inclusion of an Ir-photoredox catalyst (Figure 4.1C) within this system, while not necessary for turnover, enhances the yields and rates of NH_3 generation.

For our present catalysis system, we noted that a photoreduction step from the excited state of HEH_2, $[HEH_2]^*$, liberates the ground state radical cation $HEH_2^{\bullet+}$, which is a sufficiently strong oxidant (E_{red} = 0.48 V vs $Fc^{+/0}$) to be deleterious to N_2R.[18] We therefore reasoned that inclusion of a base to deprotonate $HEH_2^{\bullet+}$ (pK_a ~ −1) would be prudent.[18] However, the presence of a moderate Brønsted acid is typically required for chemically driven N_2R, suggesting a buffered system might be needed. A collidine/collidinium (abbreviated Col/$[ColH]^+$; Col = 2,4,6-trimethylpyridine) mixture was chosen as Col will readily deprotonate $HEH_2^{\bullet+}$ while $[ColH]^+$, with a pK_a of 15 in MeCN,[22] has been previously shown to be compatible with chemically driven N_2R using $(PNP)MoBr_3$ as a pre-catalyst (PNP = 2,6-bis(di-tert-butylphosphinomethyl)pyridine) with $(Cp^*)_2Co$ ($E_{1/2}(Co^{III/II})$ = −1.91 V; Cp* = pentamethylcyclopentadienyl) as the reductant.[21,23]

4.2 Results

Entry	Change from "standard conditions"	NH_3 (equiv/ Mo)	NH_3 yield/ HEH_2 (%)
1	none	9.5 ± 1	26.5 ± 3
2	0.57 mM Mo	21.8 ± 0.8	15.1 ± 0.6
3	no Mo	<0.1	<0.3
4	no light	<0.1	<0.3
5	no buffer	0.9 ± 0.2	2.6 ± 0.5
6	5 equiv Col/[ColH]OTf	2.9 ± 0.2	8.0 ± 0.6
7	benzene instead of THF	4.7 ± 0.1	13 ± 0.3
8	216 equiv Col/[ColH]OTf	20.3 ± 1.1	56 ± 3
9	10 equiv [TBA]Br	8.8 ± 0.3	23.6 ± 0.8
10	with $[Ir]BAr^F_4$	24 ± 4	67 ± 10
11	with $[Ir]BAr^F_4$, 5 equiv Col/[ColH]OTf	15.8 ± 0.8	44 ± 2
12	with $[Ir]BAr^F_4$, t = 1/2 h instead of 12 h	18.6 ± 0.9	52 ± 3
13	t = 2 h instead of 12 h	7.6 ± 2	21 ± 6
14	with $[Ir]BAr^F_4$, 5 equiv Col/[ColH]OTf, 0.57 mM Mo	26 ± 0.4	18.4 ± 0.4
15	with $[Ir]BAr^F_4$, 5 equiv Col/[ColH]OTf, no light	<0.1	<0.3
16	with $[Ir]BAr^F_4$, 5 equiv Col/[ColH]OTf, no Mo	<0.1	<0.3
17	with $[Ir]BAr^F_4$, 5 equiv Col/[ColH]OTf, no HEH_2	<0.1	<0.3
18	with $[Ir]BAr^F_4$, H_2-carrier = 9,10-dihydroacridine	6.4 ± 0.3	17.7 ± 0.8
19	with $[Ir]BAr^F_4$, H_2-carrier = 5,6-dihydrophenanthridine	4.6 ± 0.8	13 ± 2
20	with $[Ir]BAr^F_4$, H_2-carrier = 1-benzyl-1,4-dihydronicotinamide	1.2 ± 0.1	3.3 ± 0.3
21	with $[Ir]BAr^F_4$, 0.5 atm H_2, 0.5 atm N_2	14 ± 4	36 ± 9
22	with $[Ir(dF(CF_3)ppy)_2(dtbbpy)]PF_6$, t = 2 h instead of 12 h	2.2 ± 0.6	6 ± 1
23	with $[Ir]PF_6$, t = 2 h instead of 12 h	21 ± 4	58 ± 10
24	with $[Ir(p\text{-}F(Me)ppy)_2(dtbbpy)]PF_6$, t = 2 h instead of 12 h	22 ± 1	62 ± 3
25	with $Ir(ppy)_3$, t = 2 h instead of 12 h	7 ± 1	19 ± 4
26	with $[Ir]BAr^F_4$, no Col/[ColH]OTf	7.4 ± 0.4	20.7 ± 1

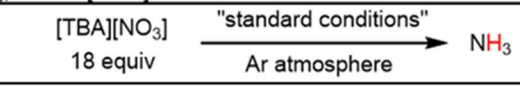

Entry	Change from "standard conditions"	NH_3 (equiv/Mo)	NH_3 yield/ HEH_2 (%)
27	none	9.8 ± 1.2	73 ± 9
28	with Mo, with $[Ir]BAr^F_4$	10.4 ± 0.5	77 ± 4
29	no Mo	1.7 ± 0.3	13 ± 2
30	no Mo, with $[Ir]BAr^F_4$	4.2 ± 1.2	31 ± 9
31	no light, with Mo, with $[Ir]BAr^F_4$	0.1 ± 0.05	0.7 ± 0.3

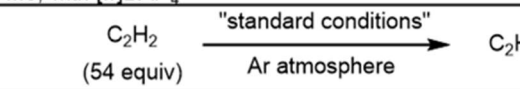

Entry	Change from "standard conditions"	C_2H_4 (equiv/Mo)	C_2H_6 (equiv/Mo)	Total yield/ HEH_2 (%)
32	none[a]	10 ± 2	1.5 ± 0.3	24 ± 5
33	with Mo,[a] with $[Ir]BAr^F_4$[b]	6 ± 1	1.1 ± 0.3	15 ± 3
34	no Mo	0.054 ± 0.008	< 0.03	< 0.3
35	no Mo, with $[Ir]BAr^F_4$[b]	2 ± 2	0.08 ± 0.08	4 ± 3
36	no light, with Mo,[a] with $[Ir]BAr^F_4$[b]	< 0.01	< 0.01	< 0.04

Table 4.1. Catalytic yields for photodriven transfer hydrogenation of N_2 to NH_3, NO_3^- to NH_3, and acetylene to ethylene and ethane . Reactions performed with 2.3 mM $[Mo]Br_3$

concentration, using a single 34 W Kessel H150 Blue lamp unless otherwise noted. All yields reported are an average of at least two runs. All runs with Ir used 2.3 mM photosensitizer loading unless otherwise noted. [a]3.6 mM [Mo]Br_3. [b]3.6 mM Ir. Ir = $[Ir(ppy)_2(dtbbpy)]BAr^F{}_4$; ppy = 2-phenylpyridinyl; dtbbpy = 4,4′-di-tert-butyl-2,2′-bipyridine; $BAr^F{}_4$ = tetrakis(3,5-bis(trifluoromethyl)phenyl)borate; dF(CF_3)ppy = 5-trifluoromethyl-2-(3,5-difluoro-phenyl)-pyridine; *p*-F(Me)ppy = 5-methyl-2-(5-fluoro-phenyl)-pyridine; PF_6^- = hexafluorophosphate).

We find that [Mo]Br_3 (1 equiv at 2.3 mM) in the presence of 54 equiv each of HEH_2, [ColH]OTf (OTf = triflate), and Col in THF, under an N_2 atmosphere and blue LED irradiation at 23 °C for 12 hours, yields 9.5 ± 1 equiv NH_3/Mo (Table 4.1, entry 1). Assuming HEH_2 is a 2 e^- donor in this process provides an NH_3 yield with respect to HEH_2 of ~25%. Use of $^{15}N_2$ confirmed N_2 as the source of the NH_3 produced (Figure C.1). To cement this interpretation, using either ^{15}N-labeled HEH_2 or ^{15}N-labeled Col/[ColH]OTf produced only $^{14}NH_3$. Analysis of the organic products following catalysis revealed complete consumption of HEH_2, with the fully oxidized Hantzsch ester pyridine (HE) as the major organic biproduct, consistent with HEH_2 acting as a 2 e^-/2 H^+ donor. We note that the yield of HE is ~90%; similarly, ~10% of the initial buffer loading is not recovered (Figure C.5). In addition to HE and recovered buffer, a complex mixture of organic species is observed following catalysis. A significant component of this mixture is generated independently via irradiation of HEH_2 and buffer in the absence of metal catalysts (Figure C.6), possibly as a result of light-induced reductive coupling as has been previously observed upon irradiation of HE in the presence of amine reductants.[24] Another factor limiting NH_3 selectivity per HEH_2 concerns background hydrogen evolution under blue light irradiation (see Figure C.8).

Higher yields of NH_3 per Mo center could be obtained by decreasing the [Mo]Br_3 loading (21.8 ± 0.8 equiv/Mo; entry 2), but with a loss in the yield of NH_3 with respect to HEH_2. The Mo-catalyst and irradiation were required to generate NH_3, and yields were substantially lower without the added buffer (entries 3-5). Attempts to use catalytic amounts of Col/[ColH]OTf (5 equiv per [Mo]Br_3) substantially lowered the NH_3 yields (entry 6). The reaction run in benzene instead of THF solvent remained catalytic but gave

attenuated yields (4.7 ± 0.1 equiv NH_3/Mo; entry 7), likely due to the lower solubility of [ColH]OTf in benzene.

While future studies are needed to probe the mechanism of this transformation, the fate of photoexcited $[HEH_2]$* is likely key. Two limiting scenarios to consider are the direct reduction of N_2R intermediates by $[HEH_2]$* (Figure C.16), or the reduction of the [ColH]OTf to $[ColH]^{\bullet}$ radical, which then reacts with $M(N_2)$ (Figure 4.2A) to form an N–H bond via $M(N_2H)$. Pyridinyl radicals have been posited as possible intermediates of N_2R in thermally driven catalysis with molecular systems.[25] Increasing the buffer concentration to 216 equiv/Mo boosted the NH_3 yield to 20.3 ± 1.1 equiv NH_3/Mo (entry 7). This observation points to a pathway whereby reduction of [ColH]OTf by $[HEH_2]$* dominates (Figure 4.2A), consistent with the high reactivity expected of $[HEH_2]$* (E_{ox} ~ –2.6 V; pK_a ~ –20; $BDFE_{C–H}$ ~ –8.5 kcal mol^{-1}), as well as its short solution lifetime (0.419 ns in DMSO solvent at 25 °C).[18,20] Accordingly, steady state-fluorimetry studies show efficient quenching of $[HEH_2]$* upon titrating in [ColH]OTf (Figure C.9). Similar titrations of Col revealed less efficient quenching (Figure C.10). However, as some NH_3 can be detected under irradiation even in the absence of buffer (entry 4), other photoinduced pathways for N–H bond formation via HEH_2 are clearly accessible. The addition of 10 equiv of tetrabutylammonium bromide (TBABr) had no effect on the NH_3 yield (entry 8), suggesting that reductive $Br^–$ loss from the precatalyst is not a limiting factor.

Figure 4.2A provides a generalized mechanistic outline to help illustrate how a photon might facilitate delivery of H_2 from HEH_2 to $M(N_2)$, to first generate an $M(NNH_2)$ intermediate, and ultimately NH_3 via successive H_2-transfers. For simplicity we show only this one scenario in Figure 4.2A but emphasize that other scenarios, including the early generation and then reduction of a terminal nitride intermediate ($Mo{\equiv}N + HEH_2 \rightarrow Mo(NH_2) + HE$) (Figure C.17), are also very plausible.[26] A recent study showed that a $Mn^V{\equiv}N$ can be photoreduced by 9,10-dihydroacridine to liberate NH_3.[27]

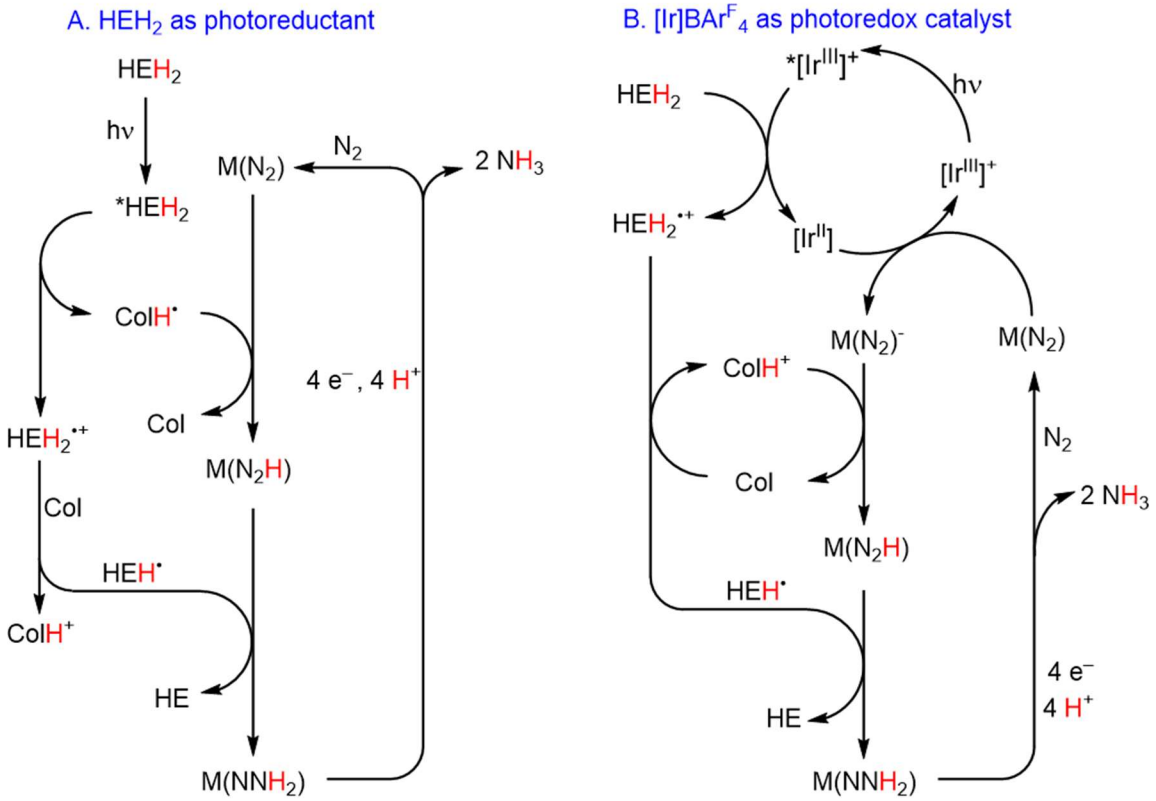

Figure 4.2. Possible scenarios for photodriven transfer hydrogenation from HEH_2 to N_2 mediated by a metal catalyst and buffer system (Col/$[ColH]^+$). (A) Scenario in absence of photoredox catalyst, in which $[HEH_2]$* is oxidatively quenched by $[ColH]^+$ to generate $[ColH]^\bullet$. (B) Scenario with photoredox catalyst, in which $[Ir^{III}]^+$* is reductively quenched by HEH_2. Pathways involving N≡N bond cleavage to yield M≡N intermediates (not shown) are also plausible (Figure C.17).

Limitations stemming from a short $[HEH_2]$* excited-state lifetime and low quantum yield (0.031)[20] for HEH_2 motivated us to explore a photosensitizer to enhance this photodriven catalysis. To test this idea, $[Ir(ppy)_2(dtbbpy)]BAr^F_4$ ($[Ir]BAr^F_4$; $E_{1/2}(Ir^{III/II})$ = −1.90 V) was chosen as its reduction potential is close to that of Cp^*_2Co and hence should be compatible with N_2R using $[Mo]Br_3$.[21,28]

Including $[Ir]BAr^F_4$ with $[Mo]Br_3$ (1 equiv, both at 2.3 mM), in addition to 54 equiv each of HEH_2 and Col/[ColH]OTf in THF, under an N_2 atmosphere and blue LED irradiation for 12 hours at room temperature, yields 24 ± 4 equiv of NH_3/Mo (entry 10). Assuming HEH_2 is a 2 e^-/2 H^+ donor, these conditions correspond to an overall NH_3 yield of 67 ± 10% with respect to HEH_2. Furthermore, in the presence of the Ir photosensitizer,

catalytic amounts of buffer can be used, producing 15.8 ± 0.8 equiv NH_3/Mo (entry 11). In addition to higher yields, the inclusion of [Ir]BAr^F_4 enhances the photocatalytic rate; the catalysis is ~80% complete after 30 minutes (entry 12). By contrast, under Ir-free conditions, 2 hour reaction times are required to achieve ~80% completion (entry 13). Comparing this photodriven Mo-catalyzed N_2R via HEH_2 with thermally driven Mo-catalyzed N_2R using $(Cp^*)_2Co$ and [ColH]OTf as reported by Nishibayashi, we find the NH_3 yields with respect to reductant to be quite similar (69% for the latter case).[21]

As in the Ir-free process, lowering the [Mo]Br_3 loading increased turnover for NH_3 with catalytic buffer (26.0 ± 0.4 equiv NH_3/Mo, entry 14), but with decreased total yield. No NH_3 is produced without irradiation (entry 16), and the presence of [Mo]Br_3 and HEH_2 are likewise essential (entries 16-17). Similar to the Ir-free reaction, HE was found to be the major organic product (>80%) and complete consumption of HEH_2 was observed. Solvent screening suggests that the reaction is most efficient when all components are soluble (see Table C.5). By contrast, other catalytic N_2R methods rely on low solubility of either the acid or reductant to attenuate competing H_2 evolution, demonstrating an advantage to using a terminal H-atom source which is not competent for H_2 release in the ground state.[1]

A range of candidate H_2-carriers should be explored in future studies to identify donors whose spent products can be recycled efficiently, perhaps *in situ*, via hydrogenation with H_2 or electrochemically (2 e^-/2 H^+). In an initial survey, the Ir-photosensitizer cocatalyst enables catalytic production of NH_3 under irradiation with 9,10-dihydroacridine or 5,6-dihydrophenanthridine as the H_2 donor (6.4 ± 0.3 equiv NH_3/Mo and 4.6 ± 0.8 equiv NH_3/Mo, respectively, entries 18-19). While non-catalytic, N_2-to-NH_3 conversion is also achieved with [Ir]BAr^F_4 and the hydride donor 1-benzyl-1,4-dihydronicotinamide (1.2 ± 0.1 equiv NH_3/Mo, entry 20). In the absence of [Ir]BAr^F_4, none of these H_2 or H^- carriers are competent for the photoinduced N_2RR (see Table C.2). The reaction with HEH_2 tolerates a 1:1 mixture of N_2 and H_2 (1 atm total pressure, 14 ± 4 equiv NH_3/Mo, entry 21), indicating that the Mo-catalyst is not (at least irreversibly) poisoned by H_2 under these conditions, important for considering downstream recycling of the spent donor.

In addition to varying the H_2-carriers we have examined the effect of varying the Ir-photosensitizer. [Ir(dF(CF_3)ppy)$_2$(dtbbpy)]PF_6 yielded substantially less NH_3 (entry 22) than [Ir]PF_6 (entry 23) or [Ir]$BAr^F{}_4$ (entries 10 and 12, Table 4.1). [Ir^{II}(dF(CF_3)ppy)$_2$(dtbbpy)] is also less reducing ($E_{1/2}(Ir^{III/II})$ = −1.75 V),[29] possibly pointing to a redox based cut-off for photodriven N_2R. Accordingly, [Ir(*p*-F(Me)ppy)$_2$(dtbbpy)]PF_6 ($E_{1/2}(Ir^{III/II})$ = −1.88 V) restores the yields observed in the parent system (entry 24).[30] However, Ir(ppy)$_3$, despite having the strongest reduction potential ($E_{1/2}(Ir^{III/II})$ = −2.57 V), gave attenuated NH_3 yields (entry 25) and therefore suggests multiple factors may be at play.

Figure 4.2B provides a working model to account for the role of [Ir]$BAr^F{}_4$. Upon excitation of $[Ir^{III}]^+$ to $[Ir^{III}]^+$*, reductive quenching by HEH_2 would generate $[Ir^{II}]$, as has been established in related reductions of organic substrates (Figure 4.2B).[9] This proposed pathway is consistent with the lack of enhancement observed with Ir(ppy)$_3$, with which reductive quenching by HEH_2 is very uphill($E_{1/2}(*Ir^{III/II})$ = −0.08 V, ($E_{1/2}(HEH_2{}^{0/+})$ = 0.48 V).[29] The resulting radical cation $HEH_2{}^{\bullet+}$ is then deprotonated by Col, mitigating back-electron transfer from $[Ir^{II}]$. As noted above, $[Ir^{II}]$ is assumed to be sufficiently reducing to generate an $M(N_2)^-$ species from $M(N_2)$. The former would then undergo protonation by $[ColH]^+$ to form an N−H bond via $M(N_2H)$, which itself can be reduced further by diffusing $HEH^\bullet$ to generate $M(NNH_2)$. As noted for Figure 4.2A, this series of steps is plausible but is only one of several related scenarios that may be viable (e.g., $[Ir^{II}]$ might be oxidized by $[ColH]^+$ instead of a [Mo]-species) and future mechanistic studies are needed.

In contrast to the Ir-free conditions, the system with the photosensitizer remains catalytically competent even without added buffer, albeit with an attenuation in turnover (7.4 ± 0.4 equiv NH_3/Mo, entry 22). Presumably, under a Col/$[ColH]^+$-free cycle, the liberated radical cation $HEH_2{}^{\bullet+}$ (formed via reductive quenching) can be consumed via proton or H-atom transfer with a [Mo]N_xH_y intermediate.

Having established photodriven transfer hydrogenation as a viable strategy for N_2R, we have begun to explore the deep reduction of other substrates. While success here will ultimately be best realized by exploring a broader array of transition metal catalysts,

promising early results with the [Mo]Br_3 catalyst discussed herein include the complete reduction of nitrate to ammonia (8 e^-/9 H^+) and acetylene to ethylene (major product, 2 e^-/2 H^+) and ethane (minor product, 4 e^-/4 H^+). These transformations have been previously explored by photochemical methods, including with semiconductors as for N_2.[31,32] Also of relevance is the photoinduced hydroalkylation of alkynes using Hantzsch ester derivatives, though transfer hydrogenation from HEH_2 to acetylene has not to our knowledge been previously reported.[33]

Reduction of [TBA]NO_3 with HEH_2 in the presence of buffer and [Mo]Br_3 under blue LED irradiation and argon atmosphere yields 9.8 ± 1.2 equiv NH_3/Mo, representing a 73 ± 9% yield with respect to HEH_2 (Table 1, entry 27). The reaction carried out with [TBA]$^{15}NO_3$ yielded $^{15}NH_3$ (Figure C.13), confirming NO_3^- as the source of N-atoms. In contrast to N_2R, addition of [Ir]$BAr^F{}_4$ did not enhance catalysis (entry 28). Distinct from N_2 as the substrate where no background reactivity is observed (entry 3), there is some background reactivity for NO_3^- even in the absence of the Mo-catalyst; this reactivity is enhanced by the Ir-photocatalyst (entries 29-30; see section C.5.5 for further discussion). Only trace NH_3 was detected in the absence of light (entry 31).

The reduction of acetylene under the same conditions (HEH_2, Col/[ColH]OTf buffer, and [Mo]Br_3 under blue LED irradiation and argon atmosphere) provides a mixture of ethylene and ethane in a ~6:1 ratio and a total yield of 24 ± 5% with respect to HEH_2 (entry 32). Addition of [Ir]$BAr^F{}_4$ to this reaction marginally decreases the yield (entry 33). However, as in the NO_3^- reduction reaction, [Ir]$BAr^F{}_4$ enhances Mo-free reactivity (entries 34-35). Again, no reduced products could be detected in the absence of light (entry 36). In sum, each of these three substrates (N_2, NO_3^-, HCCH) illustrate the capacity of HEH_2 to deliver H_2 equivalents via photodriven transfer hydrogenation.

4.3 Discussion

Reagent strengths			$BDFE_{eff}$	$\Delta\Delta G_f(NH_3)$
HEH_2 BDFE 62.3 kcal mol^{-1}	+	$HEH^{\bullet}$ BDFE 40.5 kcal mol^{-1}	51.4 kcal mol^{-1}	1.8 kcal mol^{-1}
$^{*}[HEH_2]$ E_{ox} −2.5 V	+	$ColH^{+}$ pK_a 15	15.5 kcal mol^{-1}	109 kcal mol^{-1}
$Ir^{II}(ppy)_2(dtbbpy)$ E_{ox} −1.9 V	+	$ColH^{+}$ pK_a 15	29.3 kcal mol^{-1}	68 kcal mol^{-1}

$$BDFE_{eff} = 23.06(E_{ox}) + 1.37(pK_a) + C_G \quad \text{(eqn 4.1)}$$

$$\Delta\Delta G_f(NH_3) = 3((BDFE_{H2})/2 - BDFE_{eff}) \quad \text{(eqn 4.2)}$$

Figure 4.3. Estimated $BDFE_{eff}$ values and corresponding $\Delta\Delta G_f(NH_3)$ for the transformations of interest herein. Values estimated using eqns 4.1 and 4.2.

To close, it is instructive to consider the thermodynamics of the photodriven N_2R system described here and its hypothetical dark reaction (Figure 4.1C). To do this one can compare the $BDFE_{eff}$ (Figure 4.3, eqn 4.1), a measure of the thermodynamics of H-atom transfer from a set of reagents, to the BDFE of H_2 (103.9 kcal mol^{-1}).[34,35,36] The difference between these values provides an overpotential for N_2 hydrogenation, expressed as $\Delta\Delta G_f(NH_3)$ (eqn 4.2).[37] For the dark reaction, the $BDFE_{eff}$ is the average of the first (C−H) and second (N−H) BDFE's for HEH_2 and $HEH^{\bullet}$, respectively, correlating to a very small overpotential ($\Delta\Delta G_f(NH_3)$ = 1.8 kcal mol^{-1}).[18] NH_3 synthesis via transfer hydrogenation from HEH_2 to N_2 is therefore thermodynamically comparable to N_2 hydrogenation by the Haber-Bosch process. Where the latter uses high temperature and pressure to overcome the high kinetic barrier, the photodriven process described here obtains excess driving force directly from visible light. More specifically, under conditions that exclude the photosensitizer, using the estimated excited-state reduction potential of $[HEH_2]^*$ and the pK_a of $[ColH]^+$ to estimate $BDFE_{eff}$, blue light affords access to a large added driving force ($\Delta\Delta G_f(NH_3)$ = 123 kcal mol^{-1}; Figure 4.3) to push the transfer hydrogenation forward. In the presence of the Ir-photosensitizer, a smaller but still significant driving force ($\Delta\Delta G_f(NH_3)$ = 68 kcal mol^{-1}) is available. Regardless, the key point is that light generates an overpotential from an otherwise unreactive source of 2 e^-/2 H^+ stored within HEH_2 that

is sufficient to perform, via successive transfers, a net 6 e^-/6 H^+ reduction of N_2 in the presence of an appropriate catalyst and cocatalyst buffer, with additional benefit gained from inclusion of a photoredox cocatalyst. Important future goals for the work presented here include extensive mechanistic studies as well as studies aimed at *in situ* recycling of the spent HE back to HEH_2.

4.4 Cited References

1. Chalkley, M. J.; Drover, M. W.; Peters J. C. *Chem. Rev*. **2020**. 120, 5582–5636.
2. Nishibayashi, Y. *Dalton Trans*. **2018**. 47, 11290–11297.
3. Schrock, R. R. *Angew. Chem. Int. Ed*. **2008**. 47, 5512–5522.
4. Seefeldt, L. C.; Hoffman, B. M.; Peters, J. W.; Raugei, S.; Beratan, D. N.; Antony, E.; Dean, D. R. *Acc. Chem. Res*. **2018**. 51, 2179–2186.
5. Smil, V. *Enriching the Earth: Fritz Haber, Carl Bosch, and the Transformation of World Food Production*. **2000**. MIT Press.
6. Shima, T.; Hu, S.; Luo, G.; Kang, X.; Luo, Y.; Hou, Z.; *Science* **2013**. 340, 1549–1552.
7. Yamazaki, Y.; Takeda, H.; Ishitani, O. *J. Photochem. Photobiol. C: Photochem. Rev.* **2015**. 25, 106–137.
8. Elgrishi, N.; Chambers, M. B.; Wang, X. Fontecave, M. *Chem. Soc. Rev*. **2017**. 46, 761–796.
9. Wang, P.-Z.; Chen, J.-R.; Xiao, W.-J. *Org. Biomol. Chem*. **2019**. 17, 6936–6951.
10. Chen, Q.-A.; Chen, M.-W.; Yu, C.-B.; Shi, L.; Wang, D.-S.; Yang, Y.; Zhou, Y.-G. *J. Am. Chem. Soc*. **2011**. 133, 16432–16435.
11. Abou-Elenein, G. M.; Ismail, N. A.; Mohammed, Z. F.; Fahmy, H. M.; *Egypt. J. Pharmaceutical Sci*. **1992**. 33, 953–962.
12. Comer, B. M.; Fuentes, P.; Dimkpa, C. O.; Liu, Y.-H.; Fernandez, C. A.; Arora, P.; Realff, M.; Singh, U.; Hatzell, M. C.; Medford, A. J. *Joule* **2019**. 3, 1578–1605.

13. Schrauzer, G. N.; Guth, T. D. *J. Am. Chem. Soc*. **1977**. 99, 7189–7193.
14. Edwards, J. G.; Davies, J. A.; Boucher, D. L.; Mennad, A. *Angew. Chem. Int. Ed*. **1992**. 31, 480–482.
15. Medford, A. J.; Hatzell, M. C.; *ACS Catal.* **2017**. 7, 2624–2643.
16. Brown, K. A.; Harris, D. F.; Wilker, M. B.; Rasmussen, A.; Khadka, N.; Hamby, H.; Keable, S.; Dukovic, G.; Peters, J. W.; Seefeldt, L. C.; King, P. W. *Science* **2016**. 352, 448–450.
17. Brown, K. A.; Ruzicka, J.; Kallas, H.; Chica, B.; Mulder, D. W.; Peters, J. W.; Seefeldt, L. C.; Dukovic, G.; King, P. W. *ACS Catal*. **2020**. 10, 11147–11152.
18. Shen, G.-B.; Fu, Y.-H.; Zhu, X.-Q. *J. Org. Chem*. **2020**. 85, 12535–12543.
19. Jung, J.; Kim, J.; Park, G.; You, Y.; Cho, E. J. *Adv. Synth. Catal*. **2016**. 358, 74–80.
20. Zhu, D.-L.; Wu, Q.; Li, H.-Y.; Li, H.-X.; Lang, J.-P. *Chem. – Eur. J*. **2020**. 26, 3484–3488.
21. Arashiba, K.; Eizawa, A.; Tanaka, H.; Nakajima, K.; Yoshizawa, K.; Nishibayashi, Y. *Bull. Chem. Soc. Jpn*. **2017**. 90, 1111–1118.
22. Tshepelevitsh, S.; Kütt, A.; Lõkov, M.; Kaljurand, I.; Saame, J.; Heering, A.; Plieger, P. G.; Vianello, R.; Leito, I. *Eur. J. Org. Chem*. **2019**. 2019, 6735–6748.
23. Connelly, N. G.; Geiger, W. E. *Chem. Rev*. **1996**. 96, 877–910.
24. Kano, K.; Matsuo, T. *Bull. Chem. Soc. Jpn.* **1976**. 49, 3269–3273.
25. Munisamy, T.; Schrock, R. R. *Dalton Trans*. **2011**, 41, 130–137.
26. Tanaka, H.; Arashiba, K.; Kuriyama, S.; Sasada, A.; Nakajima, K.; Yoshizawa, K.; Nishibayashi, Y. *Nature Commun*. **2014**. 5, 3737–3787.
27. Wang, D.; Loose, F.; Chirik, P. J.; Knowles, R. R. *J. Am. Chem. Soc*. **2019**. **141**, 4795–4799.
28. Slinker, J. D.; Gorodetsky, A. A.; Lowry, M. S.; Wang, J.; Parker, S.; Rohl, R.; Bernhard, S.; Malliaras, G. G. *J. Am. Chem. Soc*. **2004**. 126, 2763–2767.

29. Koike, T.; Akita, M. *Inorg. Chem. Front*. **2014**. 1, 562–576.
30. Capacci, A. G.; Malinowski, J. T.; McAlpine, N. J.; Kuhne, J.; MacMillan, D. W. C. *Nat. Chem.* **2017**. 9, 1073–1077.
31. Hirakawa, H.; Hashimoto, M.; Shiraishi, Y.; Hirai, T. *ACS Catal*. **2017**. 7, 3713–3720).
32. Boonstra, A. H.; Mutsaers, C. A. H. A. *J. Phys. Chem.* **1975**. 79, 2025–2027.
33. Zhang, Y.; Tanabe, Y.; Kuriyama, S.; Nishibayashi, Y. *Chem. – Eur. J*. **2022**. 28, e202200727.
34. Bordwell, F. G.; Cheng, J. P.; Harrelson, J. A. *J. Am. Chem. Soc*. **1988**. 110, 1229–1231.
35. Tilset, M.; Parker, V. D. *J. Am. Chem. Soc*. **1989**. 111, 6711–6717.
36. Agarwal, R. G.; Coste, S. C.; Groff, B. D.; Heuer, A. M.; Noh, H.; Parada, G. A.; Wise, C. F.; Nichols, E. M.; Warren, J. J. ; Mayer, J. M. *Chem. Rev*. **2022**. 122, 1–49.
37. Chalkley, M. J.; Peters, J. C. *Eur. J. Inorg. Chem*. **2020**. 2020, 1353–1357.